ЖЭТФ, 2014, том 146, вып. 2 (8), стр. 304–312

NORMAL PHASE AND SUPERCONDUCTING INSTABILITY IN THE ATTRACTIVE HUBBARD MODEL: A DMFT(NRG) STUDY

N. A. Kuleeva [a*], ***E. Z. Kuchinskii*** [a**], ***M. V. Sadovskii*** [a,b***]

[a] *Institute for Electrophysics, Russian Academy of Sciences, Ural Branch 620016, Ekaterinburg, Russia*

[b] *Institute for Metal Physics, Russian Academy of Sciences, Ural Branch 620990, Ekaterinburg, Russia*

Received January 10, 2014

We study the normal (nonsuperconducting) phase of the attractive Hubbard model within the dynamical mean field theory (DMFT) using the numerical renormalization group (NRG) as an impurity solver. A wide range of attractive potentials U is considered, from the weak-coupling limit, where superconducting instability is well described by the BCS approximation, to the strong-coupling region, where the superconducting transition is described by Bose condensation of compact Cooper pairs, which are formed at temperatures much exceeding the superconducting transition temperature. We calculate the density of states, the spectral density, and the optical conductivity in the normal phase for this wide range of U, including the disorder effects. We also present the results on superconducting instability of the normal state dependence on the attraction strength U and the degree of disorder. The disorder influence on the critical temperature T_c is rather weak, suggesting in fact the validity of Anderson's theorem, with the account of the general widening of the conduction band due to disorder.

DOI: 10.7868/S0044451014080094

1. INTRODUCTION

The study of superconductivity in the strong-coupling region attracts theorists for a rather long time [1], and the most important advance here was made by Nozieres and Schmitt–Rink [2], who proposed an effective approach to describe crossover from the weak-coupling BCS limit to the picture of Bose–Einstein condensation (BEC) of preformed Cooper pairs in the strong-coupling limit. The recent progress in experimental studies of ultracold gases in magnetic and optical traps, as well as in optical lattices, allowed a controlled change of parameters, such as the density and interaction strength (see reviews [3, 4]), increasing the theoretical interests in studies of superfluidity (superconductivity) in the case of a very strong pairing interaction, as well as in the BCS–BEC crossover region. Probably, the simplest model allowing theoretical studies of the BCS–BEC crossover is the attractive Hubbard model. It is widely used also for the studies of the superconductor–insulator transition (see a review in [5]). The most effective modern approach to the solution of the Hubbard model, both for strongly correlated electronic systems (SCES) with repulsive interaction and for the studies of the BCS–BEC crossover in the case of attraction, is the dynamical mean field theory (DMFT), giving an exact solution in the limit of infinite dimensions [6–8]. The attractive Hubbard model was studied within the DMFT in a number of recent papers [9–12]. However, only few results were obtained for the normal (nonsuperconducting) phase of this model, for example, there were practically no studies of two-particle properties, such as the optical conductivity.

To describe the electronic properties of SCES, we obviously need to take different additional interactions, which are inevitably present in such systems into account (electron–phonon interaction, scattering by fluctuations of different order parameters, disorder scattering, etc.). Recently, we have proposed the generalized DMFT+Σ approach [13–16], which is very convenient and effective for the studies of such additional interactions (external with respect to the Hub-

*E-mail: strigina@iep.uran.ru
**E-mail: kuchinsk@iep.uran.ru
***E-mail: sadovski@iep.uran.ru

bard model itself, e. g., pseudogap fluctuations [13–16], disorder [17, 18], and electron–phonon interaction [19]). This approach was also successfully extended to the analysis of optical conductivity [17, 20]. In this paper, we apply the DMFT+Σ approach to the studies of the normal-state properties of the attractive Hubbard model, including the effects of disorder.

2. THE BASICS OF THE DMFT+Σ APPROACH

In the general case, we consider the nonmagnetic Hubbard model with site disorder. The Hamiltonian of this model can be written as

$$H = -t \sum_{\langle ij \rangle \sigma} a^{\dagger}_{i\sigma} a_{j\sigma} + \sum_{i\sigma} \epsilon_i n_{i\sigma} + U \sum_i n_{i\uparrow} n_{i\downarrow}, \quad (1)$$

where $t > 0$ is the transfer integral between nearest sites of the lattice, U is the onsite interaction ($U < 0$ in the case of attraction), $n_{i\sigma} = a^{\dagger}_{i\sigma} a_{i\sigma}$ is onsite electron number operator, $a_{i\sigma}$ ($a^{\dagger}_{i\sigma}$) is the annihilation (creation) operator for the electron with spin σ on site i, and local energy levels ϵ_i are assumed to be independent random variables at different lattice sites. To simplify the diagram technique in what follows, we assume the Gaussian distribution of these energy levels:

$$\mathcal{P}(\epsilon_i) = \frac{1}{\sqrt{2\pi}\Delta} \exp\left(-\frac{\epsilon_i^2}{2\Delta^2}\right). \quad (2)$$

The parameter Δ represents the measure of disorder, and this Gaussian random field (with the "white noise" correlation on different lattice sites) generates "impurity" scattering and leads to the standard diagram technique for the calculation of ensemble-averaged Green's functions [21].

The generalized DMFT+Σ approach [13–16] extends the standard DMFT [6–8] by introducing an additional "external" self-energy $\Sigma_{\mathbf{p}}(\varepsilon)$ (in the general case, momentum dependent), which is due to some interaction mechanism outside the DMFT. It gives an effective procedure to calculate both single- and two-particle properties [17, 20]. The success of this approach is connected with the choice of the single-particle Green's function in the form

$$G(\varepsilon, \mathbf{p}) = \frac{1}{\varepsilon + \mu - \varepsilon(\mathbf{p}) - \Sigma(\varepsilon) - \Sigma_{\mathbf{p}}(\varepsilon)}, \quad (3)$$

where $\varepsilon(\mathbf{p})$ is the "bare" electronic dispersion, while the total self-energy neglects the interference between the Hubbard and "external" interaction and is given by the additive sum of the DMFT local self-energy $\Sigma(\varepsilon)$ and the "external" self-energy $\Sigma_{\mathbf{p}}(\varepsilon)$. This preserves the standard structure of DMFT equations [6–8]. But there are two important differences from the standard DMFT. At each iteration of the DMFT cycle, we recalculate the "external" self-energy $\Sigma_{\mathbf{p}}(\varepsilon)$ using some approximate scheme for the description of "external" interaction, and the local Green's function is "dressed" by $\Sigma_{\mathbf{p}}(\varepsilon)$ at each step of the standard DMFT procedure.

For the "external" self-energy due to disorder scattering entering the DMFT+Σ cycle below, we use the simplest approximation neglecting the diagrams with "intersecting" interaction lines, i. e., the self-consistent Born approximation. For the Gaussian distribution of site energies, it is independent of the momentum and is given by

$$\Sigma_{\mathbf{p}}(\varepsilon) \to \tilde{\Sigma} = \Delta^2 \sum_{\mathbf{p}} G(\varepsilon, \mathbf{p}), \quad (4)$$

where $G(\varepsilon, \mathbf{p})$ is the single-particle Green's function (3) and Δ is the strength of site energy disorder.

To solve the single Anderson impurity problem of DMFT, we have used the reliable algorithm of the numerical renormalization group [22], i. e., the DMFT(NRG) approach.

Within the DMFT+Σ approach, we can also investigate the two-particle properties. In particular, the real part of the dynamical (optical) conductivity has the following general expression in DMFT+Σ [17, 20]:

$$\begin{aligned} \mathrm{Re}\,\sigma(\omega) = \frac{e^2\omega}{2\pi} \int\limits_{-\infty}^{\infty} d\varepsilon \, [f(\varepsilon_-) - f(\varepsilon_+)] \times \\ \times \mathrm{Re} \left\{ \phi_{\varepsilon}^{0RA}(\omega) \left[1 - \frac{\Sigma^R(\varepsilon_+) - \Sigma^A(\varepsilon_-)}{\omega}\right]^2 - \right. \\ \left. - \phi_{\varepsilon}^{0RR}(\omega) \left[1 - \frac{\Sigma^R(\varepsilon_+) - \Sigma^R(\varepsilon_-)}{\omega}\right]^2 \right\}, \quad (5) \end{aligned}$$

where e is electronic charge, $f(\varepsilon_{\pm})$ is the Fermi distribution for $\varepsilon_{\pm} = \varepsilon \pm \omega/2$, and

$$\begin{aligned} \phi_{\varepsilon}^{0RR(RA)}(\omega) = \\ = \lim_{q \to 0} \frac{\Phi_{\varepsilon}^{0RR(RA)}(\omega, \mathbf{q}) - \Phi_{\varepsilon}^{0RR(RA)}(\omega, 0)}{q^2}, \quad (6) \end{aligned}$$

where the two-particle Green's functions $\Phi_{\varepsilon}^{0RR(RA)}(\omega, \mathbf{q})$ contain all vertex corrections from the "external" interaction, but do not include vertex corrections from the Hubbard interaction. This considerably simplifies calculations of optical conductivity within the DMFT+Σ approximation, because we only have to solve the single-particle problem determining

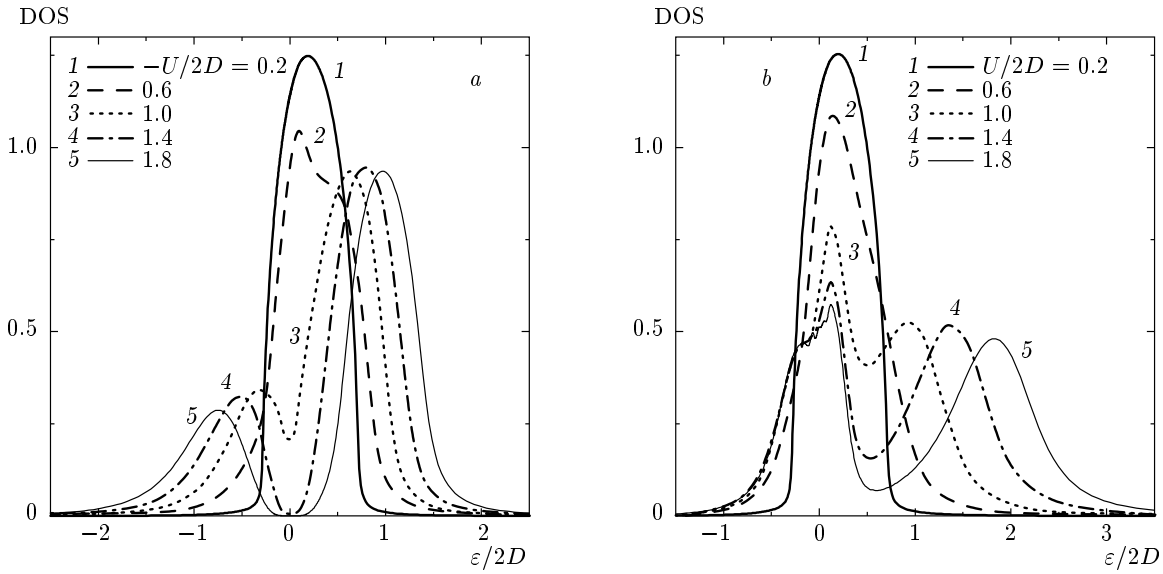

Fig. 1. Densities of states for different values of (a) Hubbard attraction and (b) repulsion. Temperature $T/2D = 0.05$

the local self-energy $\Sigma(\varepsilon_\pm)$ via the DMFT+Σ procedure. The nontrivial contribution from nonlocal correlations enters only via $\Phi_\varepsilon^{0RR(RA)}(\omega, \mathbf{q})$, which can be calculated in an appropriate approximation, taking only the "external" interaction into account. To obtain the loop contributions $\Phi_\varepsilon^{0RR(RA)}(\omega, \mathbf{q})$, determined by disorder scattering, we can either use the "ladder" approximation in the case of weak disorder, or, following Ref. [17], use the generalization of the self-consistent theory of localization [23, 24], which allows treating the case of sufficiently strong disorder. In this approach, the conductivity is determined mainly by the generalized diffusion coefficient obtained from the generalization of the self-consistency equation [23, 24] of this theory, which is to be solved in combination with the DMFT+Σ procedure.

In what follows, we consider the three-dimensional system with a "bare" semi-elliptic density of states (per elementary cell and one spin projection), which is given by

$$N_0(\varepsilon) = \frac{2}{\pi D^2}\sqrt{D^2 - \varepsilon^2} \tag{7}$$

with the bandwidth $W = 2D$. All calculations below are done for a quarter-filled band ($n = 0.5$). The value of conductivity on all figures is given in universal units $\sigma_0 = e^2/ha$ (where a is the lattice spacing).

3. MAIN RESULTS

In Fig. 1, we show the densities of states obtained for $T/2D = 0.05$ and quarter filling of the band ($n = 0.5$) for different values of the attractive ($U < 0$, Fig. 1a) and repulsive ($U > 0$, Fig. 1b) interaction. It is well known that at half-filling ($n = 1$), the density of states of the attractive and repulsive Hubbard models coincide (due to the exact mapping of these models onto each other). This is not so when we deviate from half-filling. From Fig. 1, we can see that the density of states close to the Fermi level decreases as U increases, for both attraction (Fig. 1a) and repulsion (Fig. 1b), but a significant increase in $|U|$ in the repulsive case leads only to the vanishing of the quasiparticle peak, and the density of states at the Fermi level becomes practically independent of U, while in the attractive case, the increase in $|U|$ leads to the superconducting pseudogap opening at the Fermi level (curve *3* in Fig. 1a); for $|U|/2D > 1.2$, we observe the full gap opening at the Fermi level (curves *4*, *5* in Fig. 1a). This gap is not related to the appearance of a superconducting state, but is due to the appearance of preformed Cooper pairs, because the temperature at which the results shown in Fig. 1 were obtained is larger than the superconducting transition temperature (cf. Fig. 7 below). Thus, we observe an important difference from the repulsive case, where the deviation from half-filling leads to a metallic state for arbitrary values of U, while the insulating gap at large U opens not at the Fermi level.

This picture of the density-of-states evolution with

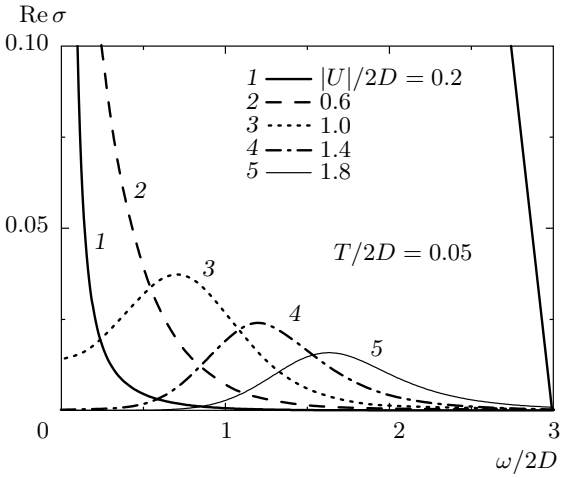

Fig. 2. Optical conductivity for different values of Hubbard attraction. Temperature $T/2D = 0.05$

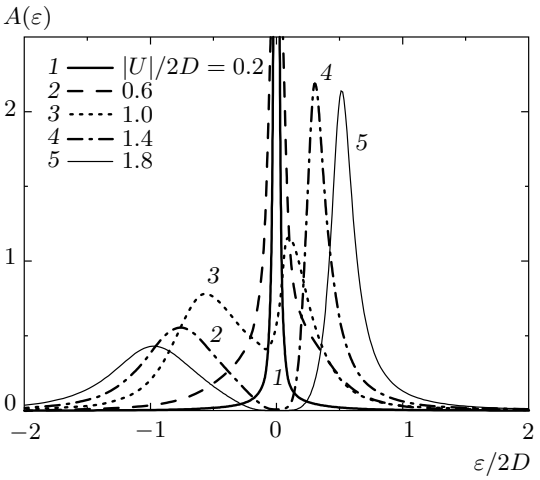

Fig. 3. Spectral density at the Fermi surface for different values of Hubbard attraction. Temperature $T/2D = 0.05$

an increase in $|U|$ is supported by the behavior of the dynamic (optical) conductivity shown in Fig. 2. We see that with an increase in $|U|$, the Drude peak at zero frequency (curves *1*, *2* in Fig. 2) is replaced by a pseudogap dip (curve *3* in Fig. 2) and the wide maximum of conductivity at a finite frequency, connected with scattering across the pseudogap. A further increase in $|U|$ leads to the appearance of the full gap in optical conductivity due to the formation of Cooper pairs (curves *4* and *5* in Fig. 2).

A similar evolution with the increase in $|U|$ is also observed in the spectral density. In Fig. 3, we show the spectral density

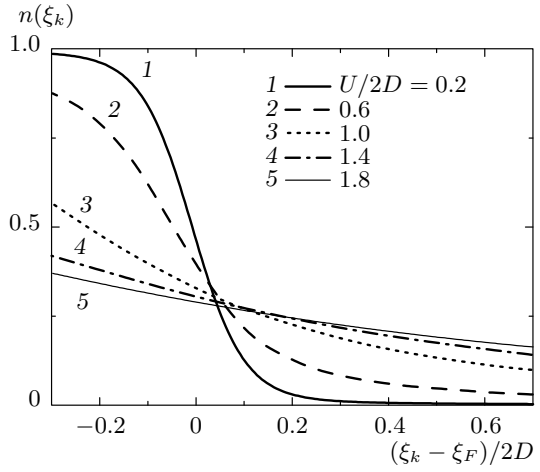

Fig. 4. Distribution function for different values of Hubbard attraction. Temperature $T/2D = 0.05$; ξ_F is the kinetic energy of electrons at the Fermi surface

$$A(\varepsilon, \mathbf{p}) = -\frac{1}{\pi} \operatorname{Im} G^R(\varepsilon, \mathbf{p})$$

at the Fermi surface ($p = p_F$) for different values of the attractive interaction U. With the increase in $|U|$, a narrow peak in the spectral density at the Fermi level (curves *1*, *2* in Fig. 3) is smeared, and with the further increase in $|U|$, the pseudogap dip appears at the Fermi level (curve *3* in Fig. 3). At still larger $|U|$, this dip is transformed into a real gap (curves *4* and *5* in Fig. 3). This behavior of the spectral density correlates well with the qualitative change (with the increase in $|U|$) of the distribution function $n(\xi_k)$ (Fig. 4), defined as

$$n(\xi_k) = \int_{-\infty}^{\infty} d\varepsilon A(\varepsilon, \xi_k) f(\varepsilon), \qquad (8)$$

where ξ_k is the kinetic energy of electrons. It can be seen that this distribution changes from a more or less defined Fermi step-function at small $|U|$ (curves *1*, *2* in Fig. 4) to an effective constant at large values of $|U|$ (curves *4* and *5* in Fig. 4), due to the formation of Cooper pairs with the binding energy of the order of $|U|$.

The formation of the superconducting pseudogap and the Cooper pairing gap with an increase in $|U|$ is also well demonstrated by the spectral density maps shown in Fig. 5 for different values of U. Color represents the spectral density intensity. We observe that the increase in $|U|$ leads to the transformation of the initially well-defined dispersion in Fig. 5*a* to dispersions with a pseudogap region, shown in Fig. 5*b*,*c*, which

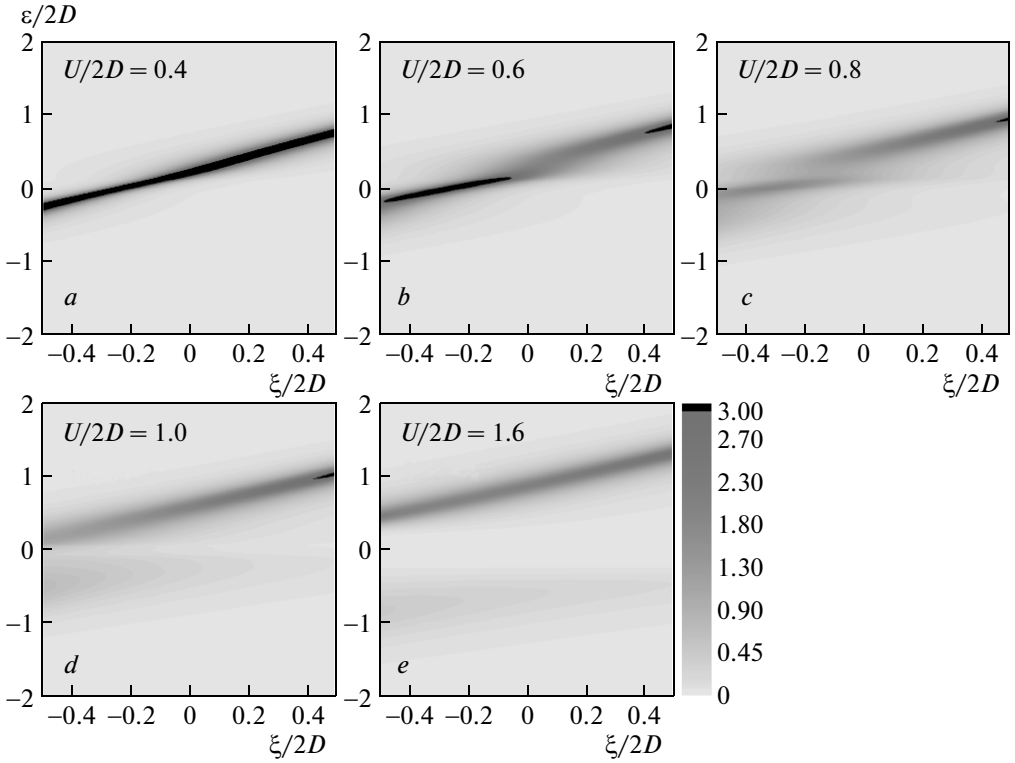

Fig. 5. Spectral density maps for different values of Hubbard attraction. Color represents the spectral density intensity. Temperature $T/2D = 0.05$

transforms into the real Cooper gap shown in Fig. 5*d*,*e* with a further increase in $|U|$.

3.1. Disorder effects

In Fig. 6, we show the evolution of the density of states and optical conductivity with changing disorder. At a sufficiently weak attraction ($|U|/2D = 0.8$, Fig. 6*a*,*b*), we see that the increase in disorder smears the density of states, leading to some widening of the band. This smearing masks the peculiarities of the density of states due to correlation effects. In particular, the quasiparticle peak and "wings" due to the upper and lower Hubbard bands observed in the density of states in Fig. 6*a* in the absence of disorder completely vanish at a sufficiently strong disorder. There are no singularities in the density of states due to the Anderson metal–insulator transition, which occurs at $\Delta/2D = 0.37$ [17], because the density of states does not feel Anderson localization. The evolution of optical conductivity with the increase in disorder Δ, shown in Fig. 6*b*, corresponds in general to the evolution of the density of states. The increase in disorder, while it remains sufficiently weak (curves *1*, *2* in Fig. 6*b*), leads to some increase in static conductivity, which is connected with the suppression of correlation effects at the Fermi level, noted above (curves *1* and *2* in Fig. 6*a*). The further increase in disorder leads to a significant widening of the band and the decrease in the density of states (curve *3* in Fig. 6*a*,*b*), which leads to a decrease in static conductivity. Finally, with the further increase in disorder, Anderson localization effects become important. At $T = 0$, the Anderson transition occurs at $\Delta/2D = 0.37$ [17]. However, we here consider the case of high enough temperature $T/2D = 0.05$, such that the static conductivity (curves *4* and *5* in Fig. 6*b*) remains finite, although we clearly observe localization behavior with $\sigma(\omega) \propto \omega^2$ at finite frequencies. At larger value of the attractive interaction $|U|/2D = 1$, the evolution of the density of states and optical conductivity is more or less similar (Fig. 6*c*,*d*). However, in the absence of disorder, we here observe a superconducting pseudogap in the density of states and the increase in disorder suppresses it, leading both to the increase in the density of states at the Fermi level and the appropriate increase in static conductivity. Finally, at a still larger attrac-

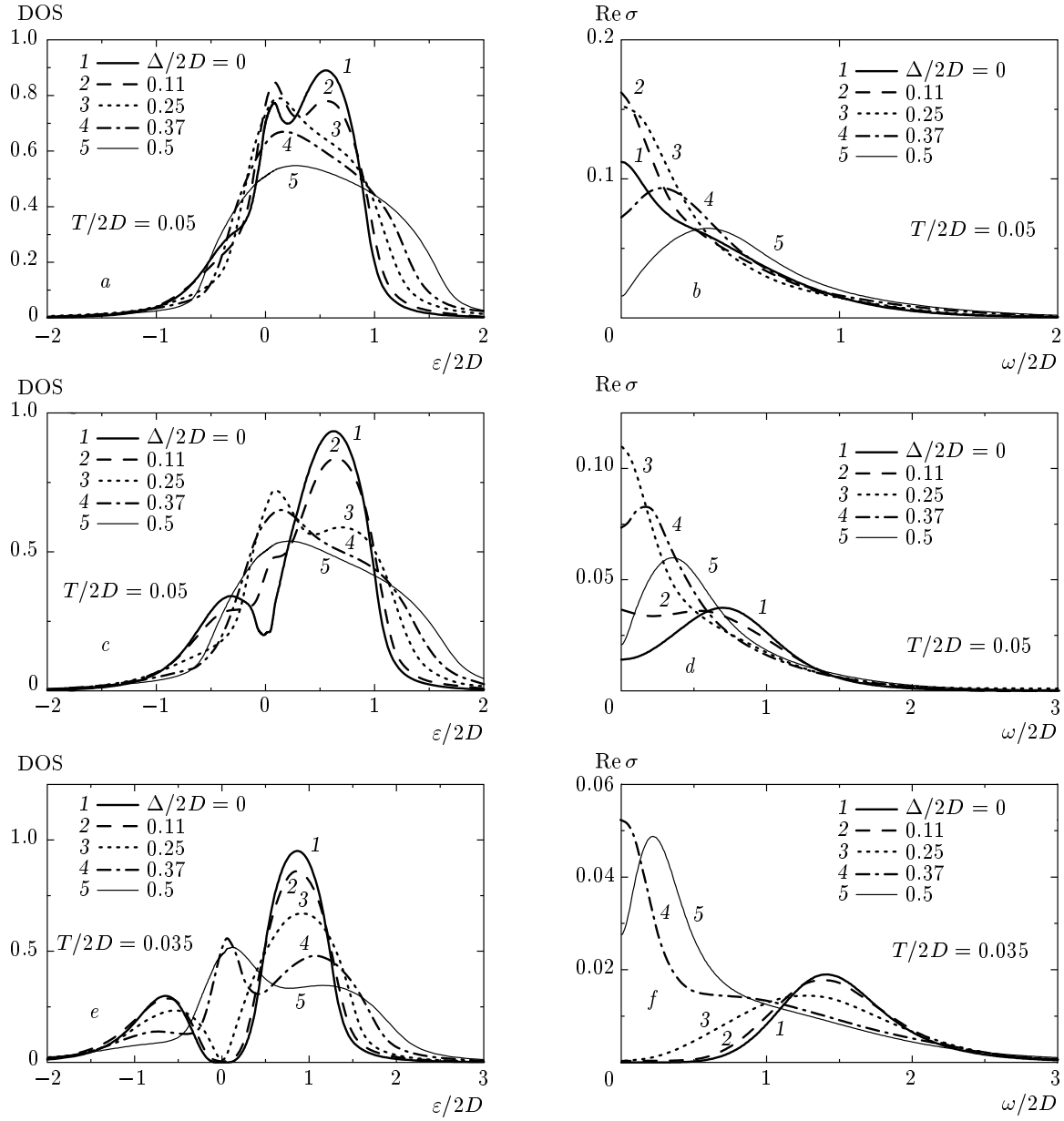

Fig. 6. Evolution of the density of states (left panels) and optical conductivity (right panels) with disorder for different values of U ((a,b) $|U|/2D = 0.8$; (c,d) $|U|/2D = 1.0$; (e,f) $|U|/2D = 1.6$)

tion $|U|/2D = 1.6$ (Fig. 6*e*,*f*) in the absence of disorder, there is a real Cooper gap in the density of states. This gap is also clearly observed in optical conductivity. With the increase in disorder, the Cooper gap both in the density of states and in conductivity becomes narrower (curves *1*–*3*). A further increase in disorder leads to the complete suppression of the Cooper gap and restoration of the metallic state with a finite density of states at the Fermi level and a finite static conductivity. This closure of the Cooper gap is related to the widening of the effective bandwidth W_{eff} due to disorder, which leads to the diminishing ratio $|U|/W_{eff}$, which controls the formation of the Cooper gap. The situation here is similar to the closure of the Mott gap by disorder in the repulsive Hubbard model [17]. However, at larger disorder (curve *5* in Fig. 6*f*), we clearly observe localization behavior, such that the increase in disorder at $T = 0$ first leads to the metallic state (the closure of the Cooper gap), while the further increase in disorder induces the Anderson metal–insulator tran-

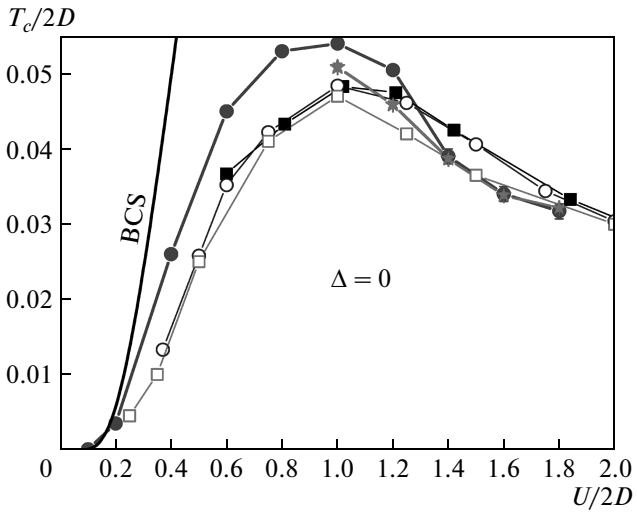

Fig. 7. Dependence of the superconducting critical temperature on the attractive interaction strength. Black squares, white circles, and white squares show the respective results in Refs. [9, 10, 12] for the quarter-filled band with $n = 0.5$. Stars represent the results obtained from the criterion of instability of the normal phase. Filled circles show T_c obtained in the Nozieres–Schmitt-Rink approximation. The continuous black curve represents the result of the BCS theory

sition. A similar picture is observed for large positive U at half-filling ($n = 1$) [17], where the increase in disorder leads to the Mott-insulator–correlated-metal–Anderson-insulator transition.

3.2. Superconducting transition temperature

The superconducting transition temperature T_c in the attractive Hubbard model was studied in a number of papers [9, 10, 12], both from the criterion of instability of the normal phase (divergence of the Cooper susceptibility) [9] and from the condition of vanishing of the superconducting order parameter [10, 12]. In Fig. 7, black squares, white circles, and white squares respectively show the results in Refs. [9, 10, 12] for quarter-filling[1)] $n = 0.5$.

Actually, the overall picture of the T_c dependence on U is well approximated by the filled-circle curve shown in Fig. 7 and obtained from the Nozieres–Schmitt-Rink [2] approach, which gives the correct (approximate) description of the BCS–BEC crossover. For the critical temperature T_c, we then have the usual BCS-like equation

$$1 = \frac{|U|}{2} \int\limits_{-D}^{D} d\varepsilon N_0(\varepsilon)(\varepsilon - \mu)^{-1} \operatorname{th} \frac{\varepsilon - \mu}{2T_c}, \qquad (9)$$

while the chemical potential for different values of U is to be determined from DMFT calculations (for a fixed band-filling). From Fig. 7, we can see that in the weak-coupling region $|U|/2D \ll 1$, the critical temperature in this approach is close to the usual result of the BCS theory (see the appropriate curve in Fig. 7). For $|U|/2D \sim 1$, the critical temperature T_c has the maximum value, while for $|U|/2D \gg 1$, it decreases as $T_c \sim 1/|U|$ [2], because for such high values of attractive interaction, the critical temperature is determined by the condition of Bose condensation of preformed Cooper pairs and the transfer amplitude of these pairs appears only in the second order of the perturbation theory and is proportional to $t^2/|U|$ [2]. Stars in Fig. 7 show the critical temperature obtained from the criterion of normal-phase instability. For large enough U, decreasing the temperature leads to an instability of the DMFT(NRG) iteration procedure: at high enough temperatures, the DMFT(NRG) procedure converges to a single solution, while for temperatures below some critical temperature, we observe two different stable solutions for odd or even iterations. We suggest that this instability of the iteration procedure corresponds to the physical instability of the normal phase. Unfortunately, for $|U|/2D < 1$, the observed instability is rather weak (the difference between the odd and even iterations is too small), and hence the accuracy of our calculations is insufficient to determine T_c in this way. Surprisingly enough, the results for T_c obtained from the approximate approach in Ref. [2] and from the instability of the DMFT(NRG) cycle are rather close to each other. This is especially surprising for large values of the $U/2D$ ratio, where the pseodigap (or even the real gap) develops in the density of states.

In Fig. 8, we show the dependence of the critical temperature, obtained from the criterion of normal state instability, on the disorder strength Δ for $|U|/2D = 1.6$. At small Δ, we observe a weak suppression of T_c by disorder, which is apparetnly due to the general smearing of the density of states and bandwidth widening by disorder scattering. At large enough disorder, we observe a significant increase in T_c with the increase in Δ. This is related to the increase in the effective bandwith W_{eff} due to disorder, leading to an effective increase in the ratio $|U|/W_{eff}$, controlling the value of the critical temperature in this model. The

[1)] In Ref. [10], it was claimed that $n = 0.75$ was considered, but the results obtained practically coincide with those in Ref. [9] obtained for $n = 0.5$.

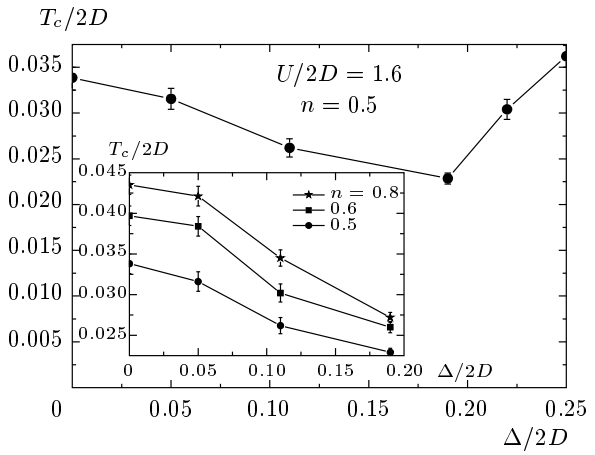

Fig. 8. Dependence of the superconducting critical temperature on disorder for $|U|/2D = 1.6$. Inset: T_c suppression by weak disorder for band-filling values $n = 0.5$, $n = 0.6$, and $n = 0.8$

increase in disorder leads to the decrease in $|U|/W_{eff}$ from 1.6 at $\Delta = 0$ to $|U|/W_{eff} \sim 1$ for $\Delta/2D \sim 0.4$, which leads to the appropriate increase in the critical temperature (cf. Fig. 7). This behavior is similar to the increase in the critical value of repulsion in the Hubbard model for the Mott metal–insulator transition with the increase in disorder (cf. Ref. [17, 18]). The decrease in $|U|/W_{eff}$ with the increase in disorder does not allow guaranteeing the sufficient accuracy of the values of T_c in the case $|U|/2D \sim 1$ for disorder values larger than $\Delta/2D = 0.11$. For such small values of disorder and for $|U|/2D \sim 1$, the critical temperature is weakly suppressed by disorder, similarly to the behavior shown in Fig. 8 for $|U|/2D = 1.6$. In the inset to Fig. 8, we show the suppression of the critical temperature by weak disorder for different band-filling values: $n = 0.5$, $n = 0.6$, and $n = 0.8$.

4. CONCLUSIONS

Within the DMFT+Σ generalization of dynamical mean field theory, we have studied the properties of the normal (nonsuperconducting) state of the attractive Hubbard model for the wide region of values of the on-site attractive interaction U. The results for the density of states, spectral density, distribution function, and dynamic (optical) conductivity demonstrate the formation of the superconducting pseudogap at the Fermi level for intermediate values of the coupling strength $|U|/2D \sim 1$ and the formation of a real Cooper gap in the strong-coupling region $|U|/2D > 1$. The appearance of a Cooper gap is related to the formation of compact Cooper pairs at temperatures that are significantly higher than the critical superconducting transition temperature T_c, which is determined as the Bose-condensation temperature of such (preformed) pairs. Within our DMFT+Σ, approach, we have also studied the influence of disorder on the properties of the normal phase. It was shown that the increase in disorder in the strong-coupling region leads to the closure of the Cooper gap and restoration of the metallic state, while in the intermediate-coupling region, disorder smears the superconducting pseudogap and increases the density of states at the Fermi level. In both cases, this is related to the general widening of the band (in the absence of U) by disorder.

We have determined the critical superconducting transition temperature T_c from the condition of instability of the normal phase. Two methods to find this instability were used, demonstrating quantitatively similar results. In the weak-coupling region, T_c is well described by the BCS theory, while in the strong-coupling region, it is related to Bose condensation of (preformed) Cooper pairs and decreases as $1/|U|$ with the increase in $|U|$, passing through the maximum at $|U|/2D \sim 1$. We have also studied the effects of disorder on T_c. It was shown that the effect of disorder on T_c is rather weak. In the strong-coupling region, e. g., for $U/2D = 1.6$, we observe both weak suppression of the critical temperature and some increase in T_c with the increase in Δ for strong enough disorder. In fact, this behavior suggests the validity of the Anderson theorem (as was conjectured for the BCS–BEC crossover region in Ref. [25]), with changes of T_c related to the widening of the conduction band by disorder. These results are also consistent with the recent lowest-order perturbation theory analysis of the effects of disorder throughout the BCS–BEC crossover region [26].

This work was supported in part by the RFBR (grant № 14-02-00065) and was performed within the Program of Fundamental Research of the Ural Branch of the Russian Academy of Sciences "Quantum macrophysics and nonlinear dynamics" (projects №№ 12-П-2-1002, 12-Т-2-1001).

REFERENCES

1. A. J. Leggett, in *Modern Trends in the Theory of Condensed Matter*, ed. by A. Pekalski and J. Przystawa, Springer, Berlin (1980).

2. P. Nozieres and S. Schmitt-Rink, J. Low Temp. Phys. **59**, 195 (1985).

3. I. Bloch, J. Dalibard, and W. Zwerger, Rev. Mod. Phys. **80**, 885 (2008).

4. L. P. Pitaevskii. Usp. Fiz. Nauk **176**, 345 (2006).

5. Yen Lee Loh, and Nandini Trivedi, arXiv:1309.4716.

6. Th. Pruschke, M. Jarrell, and J. K. Freericks, Adv. Phys. **44**, 187 (1995).

7. A. Georges, G. Kotliar, W. Krauth, and M. J. Rozenberg, Rev. Mod. Phys. **68**, 13 (1996).

8. D. Vollhardt, in *Lectures on the Physics of Strongly Correlated Systems XIV*, ed. by A. Avella and F. Mancini, AIP Conference Proceedings Vol. 1297, American Institute of Physics, Melville, New York (2010), p. 339.

9. M. Keller, W. Metzner, and U. Schollwock, Phys. Rev. Lett. **86**, 4612 (2001).

10. A. Toschi, P. Barone, M. Capone, and C. Castellani, New J. Phys. **7**, 7 (2005).

11. J. Bauer, A. C. Hewson, and N. Dupis, Phys. Rev. B **79**, 214518 (2009).

12. A. Koga and P. Werner, Phys. Rev. A **84**, 023638 (2011).

13. E. Z. Kuchinskii, I. A. Nekrasov, and M. V. Sadovskii, Pisma v Zh. Eksp. Teor. Fiz. **82**, 217 (2005).

14. M. V. Sadovskii, I. A. Nekrasov, E. Z. Kuchinskii, Th. Prushke, and V. I. Anisimov, Phys. Rev. B **72**, 155105 (2005).

15. E. Z. Kuchinskii, I. A. Nekrasov, and M. V. Sadovskii, Low Temp. Phys. **32**, 398 (2006).

16. E. Z. Kuchinskii, I. A. Nekrasov, and M. V. Sadovskii, Usp. Fiz. Nauk **182**, 345 (2012).

17. E. Z. Kuchinskii, I. A. Nekrasov, and M. V. Sadovskii, Zh. Eksp. Teor. Fiz. **133**, 670 (2008).

18. E. Z. Kuchinskii, N. A. Kuleeva, I. A. Nekrasov, and M. V. Sadovskii, Zh. Eksp. Teor. Fiz. **137**, 368 (2010).

19. E. Z. Kuchinskii, I. A. Nekrasov, and M. V. Sadovskii, Phys. Rev. B **80**, 115124 (2009).

20. E. Z. Kuchinskii, I. A. Nekrasov, and M. V. Sadovskii, Phys. Rev. B **75**, 115102 (2007).

21. A. A. Abrikosov, L. P. Gorkov, and I. E. Dzyaloshinskii, *Quantum Field Theoretical Methods in Statistical Physics*, Pergamon Press, Oxford (1965); M. V. Sadovskii, *Diagrammatics*, World Scientific, Singapore (2006).

22. R. Bulla, T. A. Costi, and T. Pruschke, Rev. Mod. Phys. **60**, 395 (2008).

23. D. Vollhardt and P. Wölfle, Phys. Rev. B **22**, 4666 (1980); Phys. Rev. Lett. **48**, 699 (1982); in *Anderson Localization*, *Springer Series in Solid State Sciences*, ed. by Y. Nagaoka and H. Fukuyama, Springer-Verlag, Berlin (1982), Vol. 39, p. 26.

24. M. V. Sadovskii, *The Theory of Electron Localization in Disordered Systems*, *Soviet Scientific Reviews–Physics Reviews*, ed. by I. M. Khalatnikov, Harwood Academic Publ., New York (1986), Vol. 7, p. 1; A. V. Myasnikov and M. V. Sadovskii, Fiz. Tverd. Tela **24**, 3569 (1982); E. A. Kotov and M. V. Sadovskii, Z. Phys. B **51**, 17 (1983).

25. A. I. Posazhennikova and M. V. Sadovskii, Pisma v Zh. Eksp. Teor. Fiz. **65**, 258 (1997).

26. F. Palestini and G. C. Strinati, arXiv:1311.2761.